

The Spatio-temporal Statistical Structure and Ergodic Behaviour of Scalar Turbulence Within a Rod Canopy

Khaled Ghannam¹ · Davide Poggi² ·
Amilcare Porporato³ · Gabriel G. Katul^{1,3}

Received: 26 February 2015 / Accepted: 9 July 2015
© Springer Science+Business Media Dordrecht 2015

Abstract Connections between the spatial and temporal statistics of turbulent flow, and their possible convergence to ensemble statistics as assumed by the ergodic hypothesis, are explored for passive scalars within a rod canopy. While complete ergodicity is not expected to apply over all the spatial domain within such heterogeneous flows, the fact that canopy turbulence exhibits self-similar characteristics at a given depth within the canopy encourages a discussion on necessary conditions for an ‘operational’ ergodicity framework. Flows between roughness elements such as within canopies exhibit features that distinguish them from their well-studied classical boundary-layer counterparts. These differences are commonly attributed to short-circuiting of the energy cascade and the prevalence of intermittent von Kármán vortex streets in the deeper layers of the canopy. Using laser-induced fluorescence measurements at two different depths within a rod canopy situated in a large flume, the spatio-temporal statistical properties and concomitant necessary conditions for ergodicity of passive scalar turbulence statistics are evaluated. First, the integral time and length scales are analyzed and their corresponding maximum values are used to guide the construction of an ensemble of independent realizations from repeated spatio-temporal concentration measurements. As a statistical analysis for an operational ergodicity check, a Kolmogorov–Smirnov test on the distributions of temporal and spatial concentration series against the ensemble was conducted. The outcome of this test reveals that ergodicity is reasonably valid over the entire domain except close to the rod elements where wake-induced inhomogeneities and damped turbulence prevail. The spatial concentration statistics within a grid-cell (square domain formed by four corner rods) appear to be less ergodic than their temporal counterparts, which is not surprising given the periodicity and persistence of von Kármán vortices in the

✉ Khaled Ghannam
khaled.ghannam@duke.edu

Gabriel G. Katul
gaby@duke.edu

¹ Nicholas School of the Environment, Duke University, Durham, NC, USA

² Dipartimento di Idraulica, Trasporti ed Infrastrutture Civile, Politecnico di Torino, Turin, Italy

³ Department of Civil and Environmental Engineering, Duke University, Durham, NC, USA

flow field. Also, a local advection velocity of dominant eddies is inferred using lagged cross-correlations of scalar concentration time series at different spatial locations. The computed probability density function of this advection velocity agrees well with the laser Doppler anemometry measurements for the same rod canopy.

Keywords Canopy turbulence · Ergodicity · Integral scales · Scalar dispersion · von Kármán streets

1 Introduction

The ergodic hypothesis was first introduced by Boltzmann in 1871 in the study of equilibrium statistical mechanics. It states that in the course of sufficiently long time, the phase trajectory of a closed system of interacting particles described by a macrostate (distribution of microstates), revisits (or passes arbitrarily close to) every phase point in the manifold (Landau and Lifshitz 1980). In other terms, the time average of some observable settles to an equilibrium value when the system ‘forgets’ its initial state, and becomes equivalent to a true (ensemble) average. In the context of turbulent flows, the ergodic hypothesis is often invoked when inquiring about the statistics of an ensemble from routinely measured temporal statistics in field or laboratory settings. In its strictest definition within the statistical fluid mechanics community, the hypothesis states that the temporal/spatial statistical moments converge to those of an ensemble of statistically stationary/homogeneous flows when the sampling is sufficiently long for the flow to experience all possible independent realizations (Monin and Yaglom 1971; Stanisic 1985). Hence, when the flow establishes a statistically steady state, temporal and/or spatial statistics of a measured turbulence quantity such as concentration converge to those of an ensemble by averaging over intervals much longer than the integral scales, provided the corresponding auto-correlation function decays to zero at finite lags (and remains so).

Numerous studies have examined the validity, or lack thereof, of the ergodic hypothesis across a wide range of turbulence problems, both theoretically and experimentally. Support for the hypothesis has been reported using direct numerical simulations (DNS) of the Navier–Stokes equations for statistically stationary and homogeneous flows (DaPrato and Debussche 2003; Galanti and Tsinober 2004). In laboratory studies, the ergodic hypothesis has also been explored using velocity time series measurements in a channel with repeated independent yet similar experiments (Lesieur 1990), while Mattingly and Weinan (2001) and Constantin et al. (2013) addressed its theoretical validity on the Navier–Stokes equations in a stochastic setting. In field measurements, Higgins et al. (2013) and Chen et al. (2014) recently examined the minimum requirements for ergodicity of atmospheric water vapor measurements over a land-lake interface and that of eddy correlation flux measurements, respectively. Nevertheless, the lack of simultaneous temporal and spatial realizations, especially inside canopies, largely limits proper testing of the validity of the ergodic hypothesis. Time averaging thus remains the common framework when reporting the statistical properties of atmospheric turbulence with spatial patterns retrieved using Taylor’s frozen turbulence hypothesis (Taylor 1938) whenever applicable (Higgins et al. 2012).

Turbulence near and within roughness elements such as canopies are drawing increased interest given their prevalence in biosphere-atmosphere studies of gas exchange (e.g. CO₂ and water vapour transport) (Finnigan 2000), ecological studies of seed and pollen spread (Nathan et al. 2002), and air quality studies such as the transport of ammonia (Sutton et al.

1995), to name a few. Turbulent flows within canopies exhibit features that distinguish them from their classical boundary-layer counterpart. The work that the flow exercises against the foliage drag produces turbulent kinetic energy (TKE) by wakes that leads to a spectral short-circuiting of the energy cascade (Finnigan 2000; Poggi et al. 2006, 2008). Previous flume and flow visualization experiments showed that the organized vortical motion within the deep layers of a rod canopy originate from quasi two-dimensional von Kármán vortex streets (Poggi et al. 2004a, b, 2011). The shedding frequency of these vortices is encoded in the classical dimensionless Strouhal number ($St = f d_r / \bar{u}$), where f is the vortex shedding frequency, d_r is a characteristic length scale of the obstacle (here rod diameter of the model canopy), and \bar{u} is the mean streamwise velocity component. The impact of the aforementioned canopy-induced phenomena on the spatio-temporal statistics and possible ergodic behaviour of passive scalar statistics remains unexplored and frames the scope of this work. The usefulness of such a discussion is evident when interpreting the statistical moments of turbulence quantities measured in laboratory and field campaigns as representative of theoretical ones, and to the subsequent comparison of such measurements with simulations or models. In essence, the gap between the temporal measurements at a point and the spatio-temporal extent of the equations of motion governing fluid flows requires an understanding of the conditions under which the two converge.

To this end, within-canopy laser induced fluorescence (LIF) measurements of dye concentration are used to examine aspects of the ergodic structure of concentration statistics at two different heights. The image processing of LIF measurements provides a practical framework for the concept of ‘similar experiments’ where spatial and temporal fields are used as proxies for multiple experiments repeated under similar external forcing. Spatial realizations at a time and temporal realizations at a point are discussed through the corresponding correlation functions, integral scales and statistical independence in comparison to characteristic time and length scales associated with physical phenomena such as the size and frequency of von Kármán vortex streets, and the mean return period of sweeping events from the canopy top. The Kolmogorov–Smirnov statistical test is used to evaluate the degree of convergence of each of the spatial and temporal statistics to those of an ensemble of realizations constructed from statistically quasi-independent events. This evaluation determines whether the constructed ensemble distribution represents a transposition of temporal to spatial statistics and vice versa. Such a transposition is also explored by computing a local eddy velocity that communicates within-canopy temporal realizations at a given location to downstream locations but with finite time lag. Using cross-correlation analysis of concentration time series at two points in the canopy space, a local advection velocity can also be retrieved and compared to published laser Doppler anemometry (LDA) measurements conducted for the same rod-canopy set-up (Poggi et al. 2004a).

2 Experimental Facilities

The data used in this work were collected from an open channel water-flow experiment with canopy-like roughness introduced as vertical rods mounted to the bottom wall of the channel. The flume configuration, the rod canopy, the acquisition of the scalar concentration time series, and the data processing are presented elsewhere (Poggi et al. 2002, 2004a, b, 2008; Poggi and Katul 2006). In brief, the experiment was carried out in a large rectangular constant head recirculating channel, 18 m long, 0.9 m wide, and 1 m deep with glass side walls to permit the passage of laser light. The rod canopy was composed of vertical stainless

steel cylinders 0.12 m tall ($=h$) and $4 \times 10^{-3}\text{ m}$ in diameter ($=d_r$), arrayed in a uniform square pattern at $n_p = 1072\text{ rods m}^{-2}$, where n_p is the canopy density defined as the number of rods per unit ground area. Using h , d_r , and n_p , the effective frontal area index is $0.81\text{ m}^2\text{ m}^{-2}$. The large n_p resulted in $C_d \approx 0.3$ comparable to those reported for agricultural crops and dense forests (Katul et al. 2004).

The local instantaneous dye concentration in a plane parallel to the channel bottom was measured using the LIF technique. The concentration measurements were conducted by (i) injecting Rhodamine 6G as a tracer, (ii) providing a horizontal light sheet between two lines of rods using a lens system, and (iii) recording a time sequence of images. The light source was provided by a 300 mW continuous fixed wavelength ion-argon laser (Melles Griot mod. 543-A-A03), and the images were recorded at a frequency of 30 Hz using a colour CCD (charge-coupled device) video camera (Poggi and Katul 2006; Poggi et al. 2006). Digital movies with a spatial resolution of $170 \times 10^{-6}\text{ m}$ were collected at two levels: $z/h = 0.2$ and $z/h = 0.5$, where z is the vertical distance referenced to the channel bottom. Three 72-s video sequences for each of the two depths were then used to compute instantaneous two-dimensional planar concentration. Throughout, the heights $z/h = 0.2$ and $z/h = 0.5$ are referred to as ‘deep’ and ‘mid-canopy’ layers. In addition, the measurements were collected at bulk canopy Reynolds numbers, $Re_* = u_*h/\nu$ of 6000 and 12,000, where $u_* = (-\overline{u'w'})^{1/2}$ is the friction velocity measured at $z/h = 1$, primed quantities are turbulent excursions, and the overbar indicates time averaging over the sampling duration. The results for the two Reynolds number were similar and the subsequent analysis uses only the $Re_* = 6000$ dataset.

It is noteworthy that, while the sampling resolution is much higher in space than in time (around 15 times), the temporal sample size is much longer and thus time statistics should have higher convergence. Figure 1 shows the ensemble-averaged temporal and spatial spectra of the measured concentration series ($z/h = 0.2$), where the latter was transformed from a wavenumber to frequency domain by the measured spatially- and temporally-averaged LDA velocity reported elsewhere (Poggi et al. 2004a). Clearly, the spatial spectrum resolves much higher frequencies than its temporal counterpart but the two have similar limited ‘scaling’ at the overlap frequency. Hence, the ensemble of spatio-temporal realizations of concentration measurements covers a wide range of turbulent scales that are not necessarily overlapping for most frequencies.

3 Methodology

Because canopy flows are inhomogeneous in z , it is unlikely that ergodicity applies in a manner similar to previously studied cases obtained for flows with homogeneous coordinates (DaPrato and Debussche 2003; Galanti and Tsinober 2004). However, connections between temporal and spatial statistics for such a complex flow may still be explored for some distance from the boundary (i.e. in a plane parallel to the mean flow at a given z/h), and at some position far from canopy elements. This is the main guiding principle for the analysis conducted here. Two different aspects of scalar concentration statistics are analyzed at each z/h : one that is based over the entire planar flow field at a certain moment in time t ; and another for one position in space over a long period of time. If canopy scalar turbulence is ergodic, these two types of statistics should converge. Lack of convergence can also be viewed as evidence against the ergodic hypothesis (operational or otherwise strict) within canopies. However,

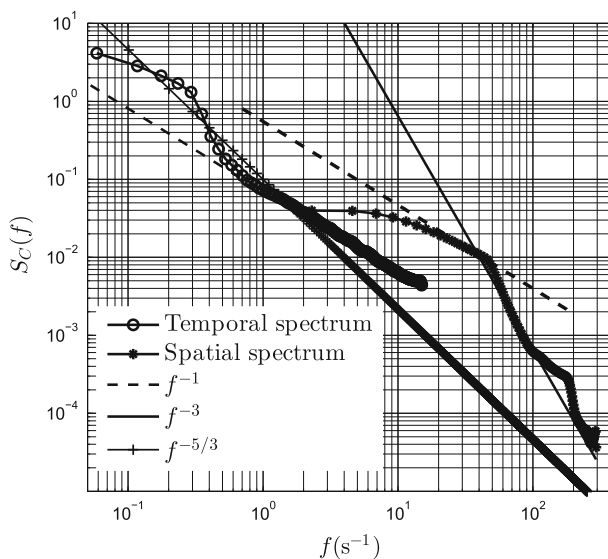


Fig. 1 Ensemble-averaged temporal (171×221 time series) and spatial (221×2100 spatial series) power spectra of concentration fluctuations. The spatial spectrum was transformed into a corresponding temporal spectrum by the relation $f = \bar{u}k$, where k is the wavenumber (inverse of spatial resolution), \bar{u} is the average streamwise velocity component ($\approx 0.1 \text{ ms}^{-1}$) and f is the frequency (s^{-1}). The linear (log scale) fits for parts of the spectra are also shown to emphasize the overlapping regions (f^{-1}). The f^{-3} scaling of the spatial spectrum reported in [Poggi et al. \(2011\)](#) and the Kolmogorov ($-5/3$) scaling are also shown. The high frequency component of the spatial spectrum reveals the effect of pixel size (high spatial resolution)

convergence of these two types of statistics cannot be used as evidence for the validity of ergodicity as such convergence is only necessary but not sufficient.

The LIF images cover one rod spacing in the streamwise direction. Hence, the spatio-temporal measurements are confined to what is referred to hereafter as the ‘one-cell configuration’—a square domain between four corner rods. This one-cell configuration occurs periodically in uniformly-spaced dense canopies, and closely resembles a domain with homogeneous coordinates for the flow field. Within this configuration, once the flow impinges on such a cell, wakes are generated behind the upstream rods and unless disrupted by a sweeping event from the canopy top, tend to grow in size until experiencing collisions with their downstream rods counterpart. It is this alternating character of persistent and spatially coherent von Kármán vortex streets and sweeping events that the current work seeks to examine as to how it alters the concentration statistics in general and necessary conditions for ‘operational’ ergodicity in particular. The spatial dimension of the planar images is 171×221 (longitudinal \times lateral) locations sampled 2100 times (around 72 s). While the same experiment is repeated three times at each of the two depths ($z/h = 0.2$ and $z/h = 0.5$), our analysis showed no significant differences among the replicates and the subsequent discussion illustrates the results from one experimental run at each of the two z/h .

The expansive dataset (array of $171 \times 221 \times 2100$) can be viewed as two configurations under similar external flow conditions (uniform water level, steady flow rate, fixed rod arrangement, and comparable initial conditions for dye releases). The first is a series of spatial realizations at each moment in time (i.e. 2100×221 spatial series each of length 171 points), while the second is 171×221 spatial locations that sample a concentration time series for about 72 s.

When discussing integral (temporal or spatial) scales of the flow, concentration excursions (C') from the local (temporal or spatial) mean are used instead of concentration differences (ΔC) so as to compare with well-established length and time scales associated with canopy turbulence and eddy sizes. Also, the maximum integral length and time scales are used as surrogates for delineating statistical independence of spatial and temporal realizations. While not necessarily exact, the choice of the maximum integral time scale (out of 171×221 available scales) to separate temporal events and maximum length scale (out of 221×2100 available scales) to separate spatial events may warrant independence. Such maximum values of length and time scales are 5–10 times their corresponding average value. When evaluating several operational aspects of ergodicity (mainly the Kolmogorov–Smirnov test for distributions), it is more convenient to consider spatial or temporal differences in LIF concentration (ΔC) (Galanti and Tsinober 2004) instead of concentration excursions from an arbitrarily set average for both configurations. The choice of concentration difference (in time or space) rather than absolute concentration excursions eliminates some potential effects of non-stationarity and inhomogeneity in the mean concentrations and dominant low frequency/wavenumber scales. Also, LIF measures light intensity rather than absolute concentration and any minor differences in background light intensity across experiments might become less relevant to concentration differences. The differencing operation itself tends to partly ‘de-correlate’ the series (at least less correlated than C') (Katul et al. 2001), which then reduces its integral scales when constructing ensembles and convergences of spatial and temporal averaging to ensembles.

Figure 2 shows typical 2-D images at the two depths during periods where the flow is dominated by von Kármán vortices along with a time series of $\partial C/\partial t \approx \Delta C/\Delta t$ and $\bar{u}\partial C/\partial x \approx \bar{u}\Delta C/\Delta x$, where \bar{u} is the measured planar- and time-averaged streamwise velocity component at the two depths (0.08 and 0.1 m s^{-1} at $z/h = 0.2$ and $z/h = 0.5$, respectively) presented elsewhere (Poggi et al. 2011). Here, $\Delta t = (1/30) \text{ s}$ and $\Delta x = 170 \times 10^{-6} \text{ m}$. The probability density functions (p.d.f.) of these series (see bottom panel of Fig. 2) exhibit a wider spread, particularly in time, relative to a standard Gaussian distribution. The discrepancies between the two distributions can be attributed to the use of the mean velocity rather than the time series of the local velocity, where the former tends to mask extreme events and therefore misses the tails in the distribution, yet constitutes the basis of Taylor’s frozen turbulence hypothesis.

4 Results and Discussion

To address the study objective, the spatio-temporal ensemble at the deep and mid-canopy layers must first be constructed from sub-sampling the differenced concentration (ΔC) series at each z/h so as to ensure replications of independent realizations. Next, the temporal p.d.f. at each location (and z/h) and the spatial p.d.f. at each moment in time (and z/h) are compared against the ensemble. It is for this reason that the integral time and length scales of C are first computed and discussed, followed by the construction of the ensembles of ΔC at each z/h . Comparisons between spatial or temporal statistics of ΔC to the constructed ensemble p.d.f. are also presented based on the Kolmogorov–Smirnov test. The transposition of spatial statistics to their temporal counterparts is further explored (at each z/h) by computing local eddy velocity that communicates time realizations at a given location to downstream locations but with finite time lag. Using cross-correlation analysis, a local advection velocity was retrieved and its statistics are compared to LDA velocity measurements conducted for the same configuration and z/h as reported elsewhere (Poggi et al. 2004a).

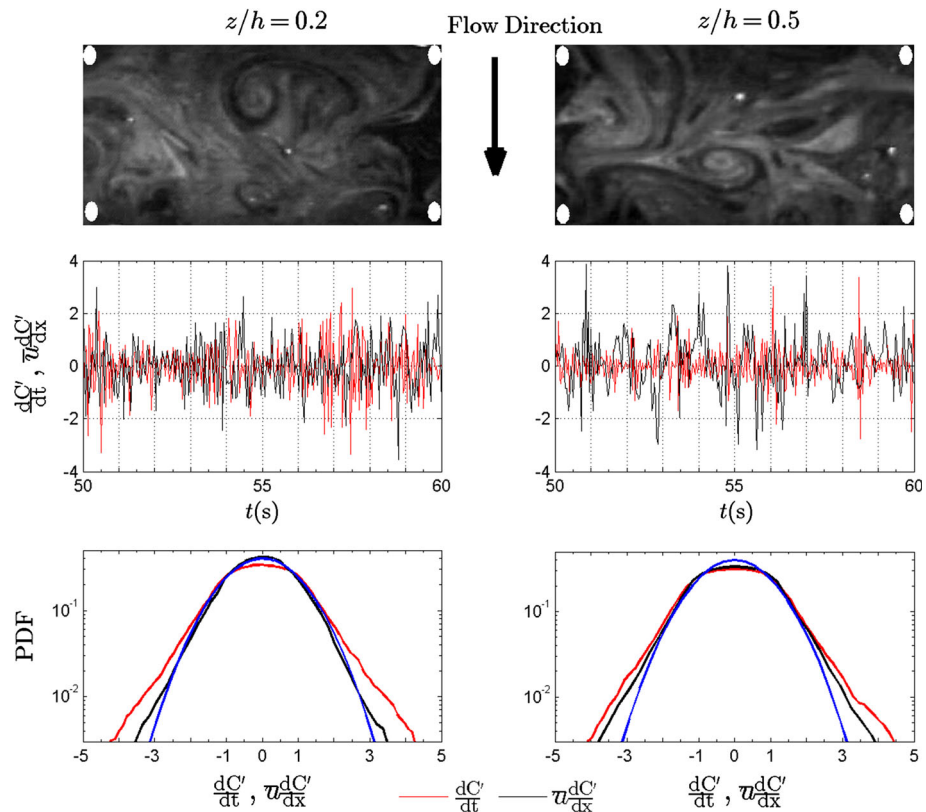


Fig. 2 Top panel 2D images of the flow field at the two depths ($z/h = 0.2$ and 0.5) during quiescent von Kármán vortex events. White circles denote rod locations. Middle panel Typical normalized time series of $\Delta C/\Delta t$ (red colour) and $\bar{u}\Delta C/\Delta x$ (black). Bottom panel The normalized p.d.f. of the time series shown in the middle panel with a Gaussian p.d.f. shown for reference (blue line)

4.1 Integral Scales

The integral time and length scales (τ and l) of C' over the spatio-temporal domain are shown in Fig. 3. For both $z/h = 0.2$ and $z/h = 0.5$, there is longer temporal memory near the obstacles compared to all downstream locations. Also, longer memory prevails in the deeper layer when compared to its mid-canopy counterpart. The maximum correlation in time was 3.2 and 1.4 s in the deep and mid-canopy layers, respectively. This result is not surprising given that the vortex streets in the deeper layer persist longer because they are less frequently disrupted by sweeping events from aloft. The latter is evident in the top panel of Fig. 3, where the integral time scale in the deep layer is comparable to h/u_* , but always smaller in the mid-canopy layer. The timescale h/u_* (≈ 2.67 s) is a measure of periodicity of sweeping events from the canopy top. To the contrary, integral length scales are somewhat larger in the mid-canopy region, while there is no difference between near-obstacle spatial correlation and elsewhere (see Fig. 3) at a given z/h . The maximum spatial correlation in the mid-canopy is around 5×10^{-3} m (rod spacing is 30×10^{-3} m and rod diameter is $d_r = 4 \times 10^{-3}$ m) and such high correlation values appear to occur during sweeping events that perturb the dominant vortical motion. In the deep layer, the integral length scale never

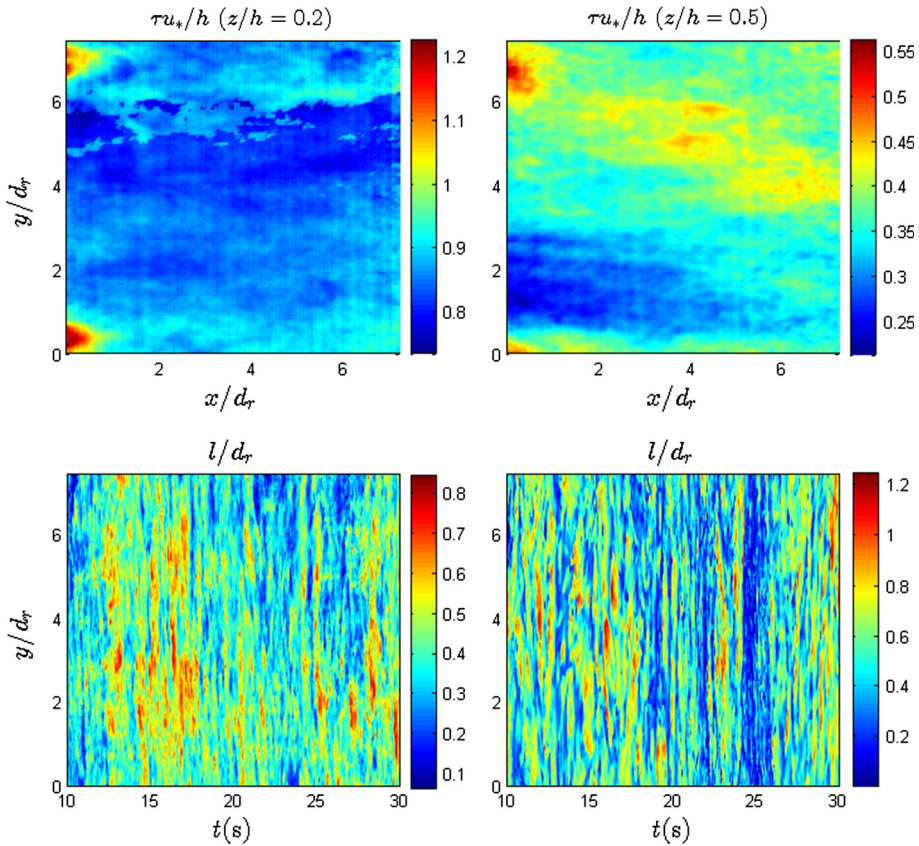


Fig. 3 Integral time (τ) and length (l) scales estimated from zero-crossings of temporal and spatial auto-correlation functions, respectively. The coordinates x and y are streamwise and lateral directions respectively. *Top panel* a total of 171×221 time series were analyzed. The flow direction is from left to right. *Bottom panel* evolution of integral length scale over a 20-s time interval. At a given time (each *image*), a total of 221 spatial series each of length 171 points downstream. τ is normalized by h/u_* and l by d_r (see text)

exceeds the rod diameter, which is a measure of the initial size of a vortex. Figure 4 shows the corresponding p.d.f. of these integral time and length scales normalized by h/u_* (where $h = 0.12$ m is the canopy height and $u_* = 0.045$ m s⁻¹ is the friction velocity at the canopy top). The time scale h/u_* often exceeds the correlation time τ in the mid-canopy layer (i.e. sweeps frequently disturb persistent vortex streets), while temporal correlations tend to persist longer.

The ensemble p.d.f. was constructed by taking a sub-sample of the ΔC dataset. This sub-set consists of all spatial and temporal ΔC realizations that are separated by the maximum auto-correlation length and time scales (inferred from C' not ΔC and calculated above), so that each point may be viewed as an independent sample. Both ensembles for the two z/h are shown in Fig. 5. The ensemble p.d.f. at $z/h = 0.2$ has a slightly heavier tail than that at $z/h = 0.5$. It is to be noted that the integral statistics of ΔC (both spatial and temporal) are much smaller than their C' counterparts, so that using the maximum integral scales of C' when constructing the ensemble ensures stronger statistical independence.

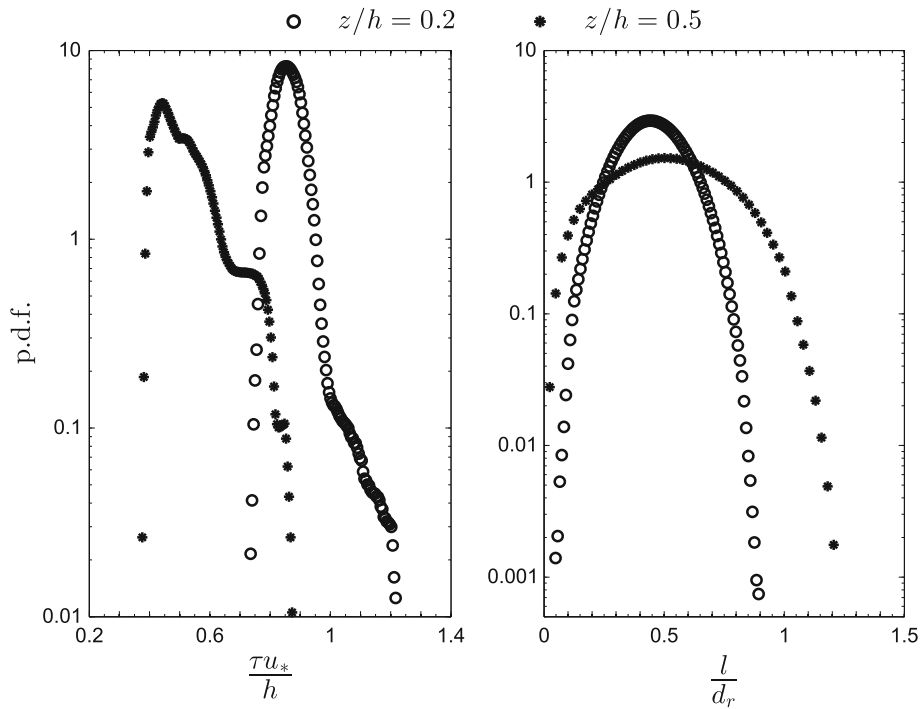


Fig. 4 The p.d.f. of the integral time and length scales shown in Fig. 3, also normalized by h/u_* and d_r respectively

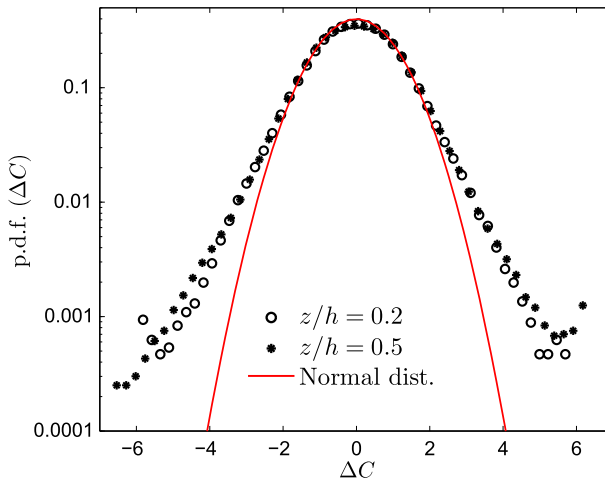


Fig. 5 The p.d.f. of the ensembles of independent spatial and temporal realizations of concentration differences at the two depths $z/h = 0.2, 0.5$, with Gaussian distribution shown for reference

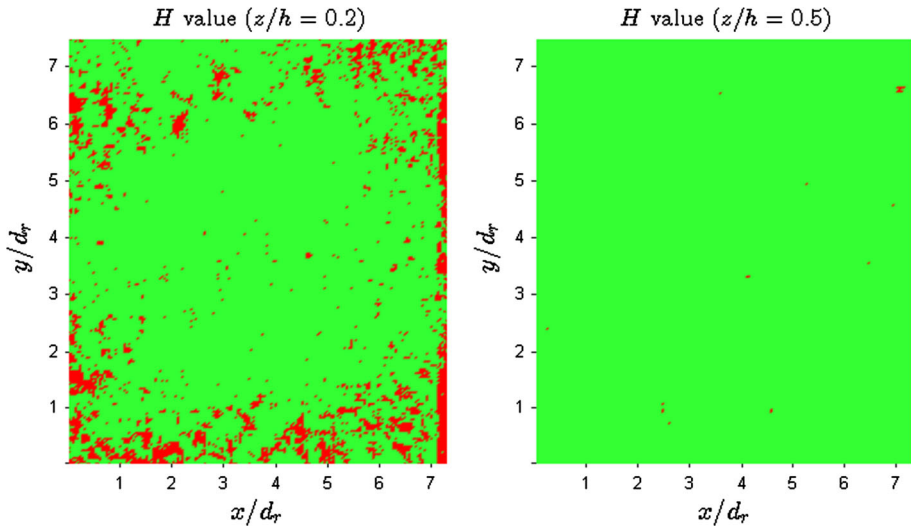


Fig. 6 Binary result of the Kolmogorov–Smirnov test when comparing the p.d.f. of each time series at each z/h against the corresponding ensemble p.d.f. The H value is binary and is either 0 (green colour indicates that the null hypothesis cannot be rejected at the 95 % confidence interval) or 1 (red colour indicates that the null hypothesis can be rejected at the 95 % confidence interval)

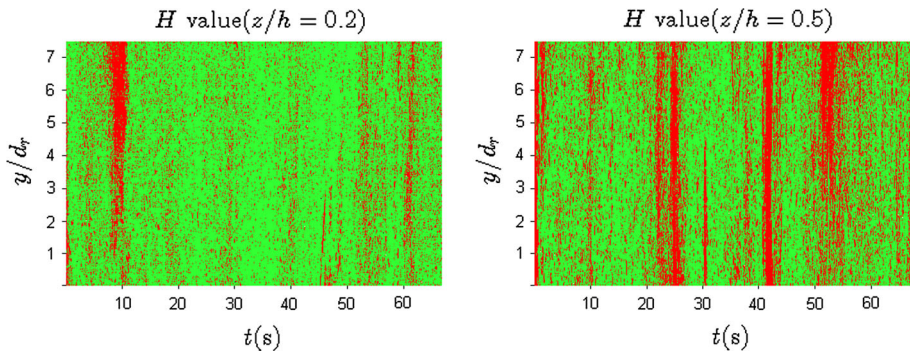


Fig. 7 Similar to Fig. 6 but for comparing the distribution of each spatial series at each depth against the corresponding ensemble distribution

4.2 Temporal and Spatial Statistics

To test the statistical similarity between the constructed ensemble and temporal distributions of concentration, the Kolmogorov–Smirnov test is performed for each time series (171×221 series) against the ensemble p.d.f. The Kolmogorov–Smirnov test is a non-parametric test that quantifies the maximum distance between the cumulative distribution functions of two samples without any prior assumptions about the distributions. The result of this test is binary (0 or 1) H values with $H = 1$ corresponding to rejecting the null hypothesis that the two p.d.f.s originate from the same distribution at the 95 % confidence level. Close to the boundary, the temporal distribution of concentration difference is not captured by the ensemble p.d.f. at $z/h = 0.2$ (Fig. 6), while all other time realizations (including higher

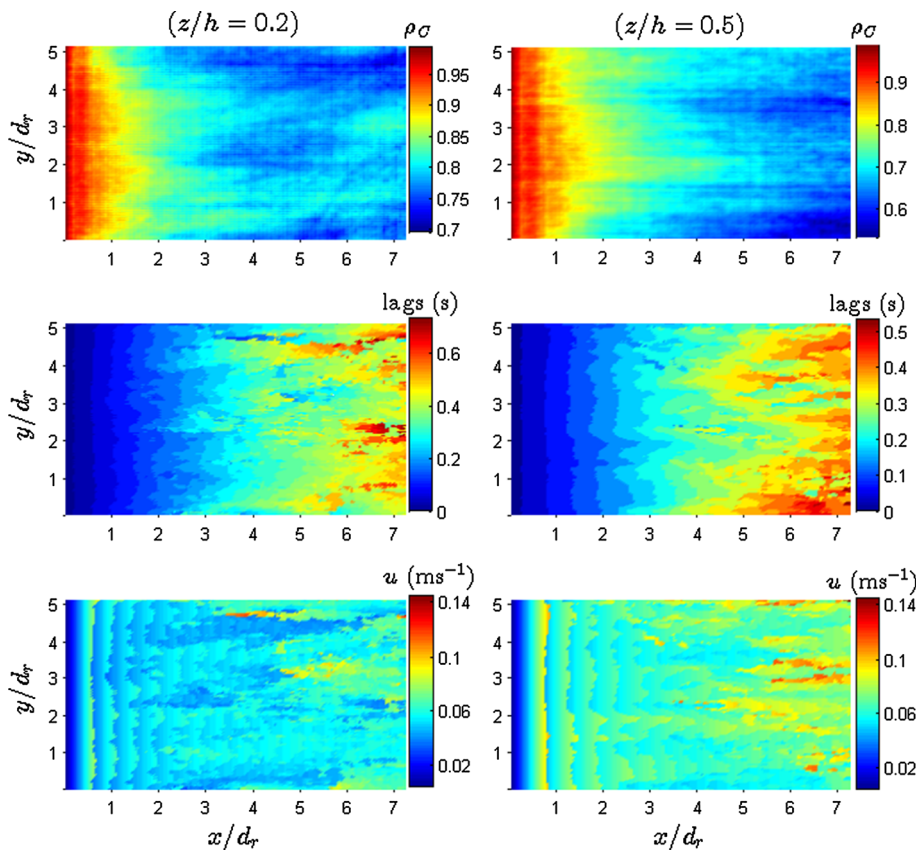


Fig. 8 Lagged cross-correlation of time series in space. *Top panel* Peak of the cross-correlation function between the concentration time series at the first location with that at all the downstream locations (170 time series). *Middle panel* time lag at which the peak in the cross-correlation function occurs. *Bottom panel* Advection velocity calculated as the ratio of the distance between the first location and any downstream location to the corresponding lag in the peak of the cross-correlation function

order statistics) are represented by this spatio-temporal transposition. Figure 6 also shows that the mid-canopy layer exhibits a stricter ergodic behaviour, where H values are almost zero everywhere. Note that while the ensemble realizations are drawn from uncorrelated (statistically independent) samples, the Kolmogorov–Smirnov test is conducted for all time series (171×221). A drawback of conducting this test on all series is that it includes some correlated events. On the other hand, the Kolmogorov–Smirnov test is being conducted on a much more expansive set of concentration differences not used in the computation of the ensemble.

Figure 7 shows the similar analysis for spatial series against the ensemble. Each point in the plot is a binary result of the Kolmogorov–Smirnov test of a spatial p.d.f. sampled at a particular time and compared to the same ensemble p.d.f. While the spatial realizations are not fully ergodic, $H = 0$ still dominates the statistical test during most times, especially in the deeper layer. The $H = 1$ regions in Fig. 7 (red colour) appear during relatively long periods of sweeping events, where the dye concentration almost approaches zero (i.e. the dye is entirely washed by sweeps). This is more evident in the $z/h = 0.5$ layer where sweeping events are more frequent.

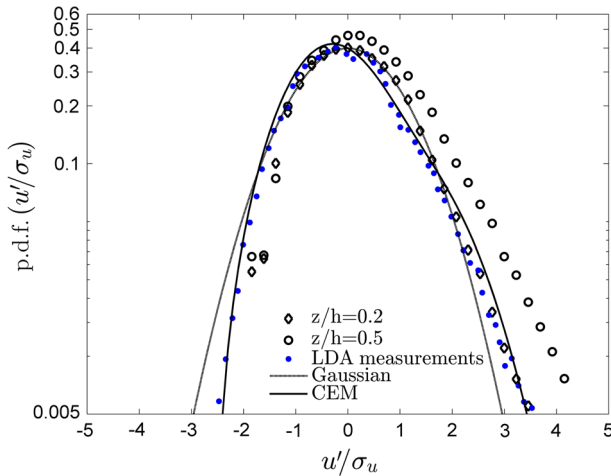


Fig. 9 The p.d.f. of the normalized advection velocity calculated from the lagged cross-correlations in Fig. 8 at $z/h = 0.2$ and $z/h = 0.5$. The reported p.d.f. of LDA-measured velocity distribution in (Poggi et al. 2004a), a third-order CEM (cumulant expansion model) fit, and Gaussian distribution are also shown for comparisons

A plausible explanation for broken ergodicity in the temporal statistics within the deeper layer (left panel of Fig. 6) and the spatial statistics in the mid-canopy layer (right panel of Fig. 7) may be attributed to the relatively larger integral time scale in the former and larger integral length scale in the latter. Such long correlation reduces the sample size of available independent realizations in time and space domains, which is missed when constructing the ensemble distribution.

4.3 Cross-Correlation and Advection Velocity

The cross-correlation function between the time series sampled at the first location (sensor) in the one cell configuration and that at all downstream locations was determined so as to compute an advection velocity that can be compared to velocity measurements conducted using the LDA. While the peak of the cross-correlation function decays with increased downstream distance, the lag (in time) at which this peak occurs increases. Figure 8 shows the results where the peak in cross-correlation function (top panel) remains significant despite decaying in space. This slow decay and finite cross-correlation indicates that the quasi-deterministic vortical structure (i.e. von Kármán streets) can expand beyond the one-cell domain and remain sufficiently coherent. For example, in the deeper layer ($z/h = 0.2$), the decrease of the cross-correlation with increasing spatial lags varies from 1 to 0.7, which is still significant. The maximum time lags are 0.7 and 0.5 s at $z/h = 0.2$ and $z/h = 0.5$, respectively. The average time for a uniform von Kármán vortex to cover a distance of one rod spacing is around 0.3 s, while the periodicity of shedding such vortices is around 0.2 s.

The advection velocity calculated from the above analysis is shown in the bottom panel of Fig. 8. On average, this calculation captures the mean streamwise velocity measured and reported by Poggi et al. (2004a) and Poggi et al. (2011) (around 0.08 and 0.1 m s⁻¹ at $z/h = 0.2$ and $z/h = 0.5$, respectively). More important here is the p.d.f. of these velocities that is shown in Fig. 9 along with the LDA velocity measurements in (Poggi et al. 2004a). The reasonable agreement here suggests that the advection velocity may be inferred from scalar concentration statistics through a spatio-temporal transposition, which is consistent with an operational view of the ergodic hypothesis.

5 Conclusion

High resolution spatio-temporal datasets of within-canopy scalar concentration measurements were collected to examine necessary conditions for ergodicity. While limited in experimental scope (due to the sampling length in time and space), the current work is the first to examine the ergodic hypothesis on scalar turbulence statistics within canopies. The main premise when analyzing this dataset is that if a turbulent flow is both statistically stationary in time and homogeneous in space, then its temporal and spatial statistical properties should be the same if the ergodic hypothesis is correct. Canopy turbulence is inhomogeneous in the vertical direction necessitating a modification to this premise. The proposed modification here replaces spatial with planar statistical properties defined at a given z/h . Even with this modification, the presence of rods may still break ergodic behaviour because canopy turbulence in the deeper layers appears to be dominated by low-dimensional (or even quasi-deterministic) motion (von Kármán vortex streets) that cannot be ergodic. However, frequent sweeps from aloft occasionally disturb the onset of such motion, and other mechanisms responsible for the breakdown of these von Kármán vortices (e.g. their subsequent collision with other rods) may produce fine-scaled turbulence that is locally homogeneous away from the rods. These other mechanisms may act to restore ergodicity but within a smaller or restricted spatial domain.

The experimental results here show a general tendency towards the validity of this operational version of the ergodic hypothesis, particularly for temporal statistics and in the mid-canopy layers where sweeps tend to frequently disturb the onset of von Kármán streets. Events associated with broken ergodicity were related to (i) sweeping and dye washing that homogenized the spatial domain (an unavoidable experimental limitation) or (ii) long memory in time near physical obstacles that prohibit proper testing of the hypothesis due to insufficient sampling of statistically independent events. However, even within the single-cell, the p.d.f. of the independently measured LDA advection velocity was reasonably recovered from cross-correlation functions of concentration time series lagged in space. This agreement suggests that the transposition of spatio-temporal scalar concentration statistics in turbulent flows within canopies can still be achieved by a local advection velocity. Hence, it can be surmised that scalar canopy turbulence does exhibit similarity between its temporal and spatial statistical properties. This transposition is deemed as necessary but not sufficient for accepting operational ergodicity within canopies.

Broader implications of these findings pertain to how the widely used combined eco-physiological and canopy transport models are compared to tower measurements. Comparisons between tower-based measurements and modeled scalar (or momentum) flux calculations are often presented using ensemble-averages, where ensemble averaging is often conducted over many days but presented by time of day (presumably reflecting similar light conditions) or by atmospheric stability class (Baldocchi and Meyers 1998; Katul and Albertson 1998). The work here suggests that such a representation may be theoretically more sound than comparisons by individual events whose duration is 30 min or so. Conducting time and some ensemble averaging over ‘similar’ conditions (be they light regimes or atmospheric stability classes) is likely to converge to the spatio-temporal average over which the combined eco-physiological and canopy transport models are derived from (if operational ergodicity is assumed). Hence, our results provide some support to the recent approaches to model-data comparisons and assessments, where ensemble averaging over similar conditions (or hydro-meteorological states) is now commonly practiced in canopy turbulence studies (but without strong rationale).

Acknowledgments Support from the National Science Foundation (NSF-AGS-1102227 and NSF-EAR-1344703), the United States Department of Agriculture (2011-67003-30222), and the U.S Department of Energy (DOE) through the Office of Biological and Environmental Research (BER) Terrestrial Carbon Processes (TCP) program (DE-SC0006967 and DE-SC0011461) is acknowledged.

References

- Baldocchi D, Meyers T (1998) On using eco-physiological, micrometeorological and biogeochemical theory to evaluate carbon dioxide, water vapor and trace gas fluxes over vegetation: a perspective. *Agric For Meteorol* 90(1):1–25
- Chen J, Hu Y, Yu Y, Lü S (2014) Ergodicity test of the eddy correlation method. *Atmos Chem Phys Discuss* 14:18207–18254
- Constantin P, Glatt-Holtz N, Vicol V (2013) Unique ergodicity for fractionally dissipated, stochastically forced 2D Euler equations. *Commun Math Phys* 46:1–39
- DaPrato G, Debussche A (2003) Ergodicity for the 3D stochastic Navier–Stokes equations. *J Math Pures Appl* 82:877947
- Finnigan J (2000) Turbulence in plant canopies. *Annu Rev Fluid Mech* 32(1):519–571
- Galanti B, Tsinober A (2004) Is turbulence ergodic? *Phys Lett A* 330:173180
- Higgins C, Froidevaux M, Simeonov V, Vercauteren N, Barry C, Parlange M (2012) The effect of scale on the applicability of Taylors frozen turbulence hypothesis in the atmospheric boundary layer. *Boundary-Layer meteorol* 143:379–391
- Higgins C, Katul G, Froidevaux M, Simeonov V, Parlange MB (2013) Are atmospheric surface layer flows ergodic? *Geophys Res Lett* 40:33423346
- Katul G, Albertson J (1998) An investigation of higher-order closure models for a forested canopy. *Boundary-Layer Meteorol* 89(1):47–74
- Katul G, Lai CT, Schäfer K, Vidakovic B, Albertson J, Ellsworth D, Oren R (2001) Multiscale analysis of vegetation surface fluxes: from seconds to years. *Adv Water Resour* 24(9):1119–1132
- Katul GG, Mahrt L, Poggi D, Sanz C (2004) One-and two-equation models for canopy turbulence. *Boundary-Layer Meteorol* 113(1):81–109
- Landau LD, Lifshitz EM (1980) Course of theoretical physics. Elsevier, Amsterdam, 537 pp
- Lesieur M (1990) Turbulence in fluids. Kluwer, Dordrecht, 367 pp
- Mattingly J, Weinan E (2001) Ergodicity for the Navier–Stokes equation with degenerate random forcing: finite-dimensional approximation. *Commun Pure Appl Math* 54:13861402
- Monin A, Yaglom A (1971) Statistical fluid mechanics: mechanics of turbulence, vol 1. MIT Press, Cambridge, 695 pp
- Nathan R, Katul GG, Horn HS, Thomas SM, Oren R, Avissar R, Pacala SW, Levin SA (2002) Mechanisms of long-distance dispersal of seeds by wind. *Nat Lett* 418(6896):409–413
- Poggi D, Katul G (2006) Two-dimensional scalar spectra in the deeper layers of a dense and uniform model canopy. *Boundary-Layer Meteorol* 121:267–281
- Poggi D, Porporato A, Ridolfi L (2002) An experimental contribution to near-wall measurements by means of a special laser Doppler anemometry technique. *Exp Fluids* 32(3):366–375
- Poggi D, Katul G, Albertson J (2004a) Momentum transfer and turbulent kinetic energy budgets within a dense model canopy. *Boundary-Layer Meteorol* 111:589–614
- Poggi D, Porporato A, Ridolfi L, Albertson J, Katul G (2004b) The effect of vegetation density on canopy sub-layer turbulence. *Boundary-Layer Meteorol* 111(3):565–587
- Poggi D, Katul G, Albertson J (2006) Scalar dispersion within a model canopy: measurements and three-dimensional Lagrangian models. *Adv Water Resour* 29(2):326–335
- Poggi D, Katul G, Cassiani M (2008) On the anomalous behavior of the Lagrangian structure function similarity constant inside dense canopies. *Atmos Environ* 42:4212–4231
- Poggi D, Katul G, Vidakovic B (2011) The role of wake production on the scaling laws of scalar concentration fluctuation spectra inside dense canopies. *Boundary-Layer Meteorol* 139(1):83–95
- Stanisic M (1985) Mathematical theory of turbulence. Springer, New York, 482 pp
- Sutton M, Schjorring J, Wyers G, Duyzer J, Ineson P, Powlson D (1995) Plant–atmosphere exchange of ammonia [and discussion]. *Philos Trans R Soc* 351(1696):261–278
- Taylor G (1938) The spectrum of turbulence. *Proc R Soc Lond Ser A* 164:476–479